

Zero-Valent Palladium Single-Atoms Catalysts Confined in Black Phosphorus for Efficient Semi-Hydrogenation

Cheng Chen, Wei Ou, Kah-Meng Yam, Shibo Xi, Xiaoxu Zhao, Si Chen, Jing Li, Pin Lyu, Lu Ma, Yonghua Du, Wei Yu, Hanyan Fang, Chuanhao Yao, Xiao Hai, Haomin Xu, Ming Joo Koh, Stephen J. Pennycook, Junling Lu, Ming Lin,* Chenliang Su,* Chun Zhang,* and Jiong Lu*

Single-atom catalysts (SACs) represent a new frontier in heterogeneous catalysis due to their remarkable catalytic properties and maximized atomic utilization. However, single atoms often bond to the support with polarized electron density and thus exhibit a high valence state, limiting their catalytic scopes in many chemical transformations. Here, it is demonstrated that 2D black phosphorus (BP) acts as giant phosphorus (P) ligand to confine a high density of single atoms (e.g., Pd₁, Pt₁) via atomic layer deposition. Unlike other 2D materials, BP with relatively low electronegativity and buckled structure favors the strong confinement of robust zero-valent palladium SACs in the vacancy site. Metallic Pd₁/BP SAC shows a highly selective semi-hydrogenation of phenylacetylene toward styrene, distinct from metallic Pd nanoparticles that facilitate the formation of fully hydrogenated products. Density functional theory calculations reveal that Pd atom forms covalent-like bonding with adjacent P atoms, wherein H atoms tend to adsorb, aiding the dissociative adsorption of H₂. Zero-valent Pd in the confined space favors a larger energy gain for the synthesis of partially hydrogenated product over the fully hydrogenated one. This work provides a new route toward the synthesis of zero-valent SACs on BP for organic transformations.

1. Introduction

Single atom catalyst (SAC) has drawn an intensive research interest in heterogeneous catalysis because of its unique catalytic properties and maximized atom efficiency.^[1–17] However, the electronic hybridization and polarization between single atoms and support often leads to a high valence state of supported single metal atoms, which significantly limit their catalytic applications in a variety of chemical conversions.^[18–20] Molecular phosphorus ligands with low electronegativity and versatile coordination ability have been widely used to synthesize zero-valent metal-complex compounds as efficient homogenous catalysts for various organic transformations.^[21–24] Inspired by this, we discovered that 2D BP with buckled structure can be viewed as a giant phosphorus ligand to anchor

C. Chen, K. M. Yam, J. Li, P. Lyu, Y. Wei, H. Y. Fang, C. H. Yao, X. Hai, H. M. Xu, M. J. Koh, C. Zhang, J. Lu
Department of Chemistry
National University of Singapore
3 Science Drive 3, Singapore 117543, Singapore
E-mail: phyzc@nus.edu.sg; chmluj@nus.edu.sg
C. Chen
NUS (Suzhou) Research Institute
No. 377 Linqun Street, Suzhou Industrial Park, Suzhou
Jiangsu 215028, China
W. Ou, X. Hai, C. L. Su
SZU-NUS Collaborative Center
International Collaborative Laboratory of 2D Materials for
Optoelectronic Science & Technology of Ministry of Education
Engineering Technology Research Center for 2D Materials Information
Functional Devices and Systems of Guangdong Province
Institute of Microscale Optoelectronics
Shenzhen University
Shen Zhen 518060, China
E-mail: chmsuc@szu.edu.cn
K. M. Yam, J. Li, H. M. Xu, C. Zhang, J. Lu
Centre for Advanced 2D Materials and Graphene Research Centre
National University of Singapore
Singapore 117546, Singapore

K. M. Yam, C. Zhang
Department of Physics
National University of Singapore
2 Science Drive 3, Singapore 117542, Singapore
S. B. Xi
Institute of Chemical and Engineering Sciences
A*STAR (Agency for Science, Technology and Research)
1 Pesek Road, Jurong Island, Singapore 627833, Singapore
X. X. Zhao
School of Materials Science and Engineering
Nanyang Technological University
Singapore 639798, Singapore
S. Chen, J. L. Lu
Department of Chemical Physics
University of Science and Technology of China
Hefei 230026, China
L. Ma, Y. H. Du
National Synchrotron Light Source II
Brookhaven National Laboratory
Upton, NY 11973, USA

DOI: 10.1002/adma.202008471

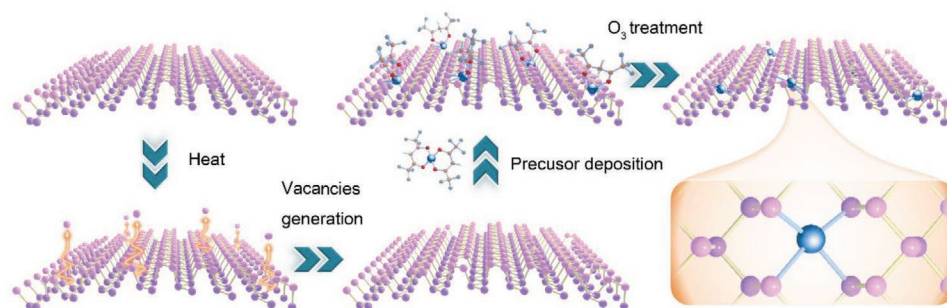


Figure 1. Schematic illustration of the synthesis of BP confined SACs via ALD. Three major steps involved in the synthetic route: i) exfoliated few-layer BP flakes were heated up to 150 °C in ALD chamber to remove the possible surface adsorbents and to generate extra vacancies as the anchor sites; ii) Subsequently, metal organic precursors are deposited and anchored in the vacancy sites of BP flakes through the partial removal of organic ligands; iii) the removal of the remaining ligands of deposited metal precursors via a further ozone (O_3) treatment at 150 °C. Palladium (II) hexafluoroacetylacetonate ($Pd(hfac)_2$) and Trimethyl(methylcyclopentadienyl)-platinum (IV) ($MeCpPtMe_3$) are used as the precursors for the synthesis of Pd_1/BP and Pt_1/BP , respectively. The balls in pink and purple represent phosphorus in top layer and bottom layer, respectively. The ball in blue represents the metal atom. The balls in red, yellow, and grey represents the oxygen, carbon, and hydrogen atoms, respectively.

various single-metal atoms with tunable electronic and catalytic properties.^[25–27] Unlike other planar 2D materials such as graphene and C_3N_4 , and MoS_2 , the intrinsic coordination properties of phosphorus atoms with a relatively low electronegativity in BP potentially render them as an ideal platform to support low-valence single-metal atoms without additional heteroatom doping.^[14] Moreover, the peculiar puckered structure of BP not only provides a cage-like coordination environment to bond single atoms in the confined space but also offers new advantages to enable unique selectivity and activity in catalysis.^[28]

Here, we demonstrated the rational synthesis of BP supported SACs (e.g., Pd_1 , Pt_1) with a controllable high loading via the atomic layer deposition (ALD). It is found that Pd atoms are anchored in the divacancy of BP via covalent bonding with the zero-valent state, as confirmed by both experimental and theoretical calculations. In contrast, Pt atoms anchored in the vacancy are prone to bond with two additional oxygen atoms, leading to a high valence state. Zero-valent Pd_1/BP SAC shows an excellent selectivity and activity in the partial hydrogenation of phenylacetylene into styrene, distinct from metallic Pd nanoparticles that promote the formation of fully hydrogenated products.

2. Results

In contrast to wet-chemical methods, ALD offers a high-precision and controllable synthesis of atomically dispersed SACs through self-limiting surface reactions.^[7,12,29,30] Therefore, we used this technique to fabricate high-loading SACs ($M = Pd$, Pt) on few-layer BP flakes obtained by electrochemical exfoliation reported in our previous work (refer to Section S1 and Figure S1, Supporting Information).^[31] Figure 1 illustrates three major steps involved in the synthetic route. Prior to the deposition of metal precursor molecules, exfoliated BP flakes were heated up to 150 °C in ALD chamber to remove the possible surface adsorbents. In addition, thermal annealing in this temperature region also facilitate the formation of extra vacancies as the anchor sites as supported by our scanning tunneling microscopy study of bulk BP (Figures S2,S3, Supporting Information).^[32,33] Subsequently, metal organic precursors are deposited and anchored in the vacancy sites of BP flakes to form the metal-phosphorus bonding through the partial removal of organic ligands. Finally, a further ozone (O_3) treatment of these samples allows for the removal of the remaining ligands of deposited metal precursors to expose the anchored single atoms on BP. In addition, the loading of isolated metal atoms can be precisely tuned by controlling the exposure time to precursors. The maximal loading of SACs can be achieved once all the anchor sites are fully utilized, beyond that the nanoparticles will form (Figures S4–S6, Supporting Information).^[34–36] The maximal loading of Pt_1/BP and Pd_1/BP obtained (the exposure time of 60 s) is determined to be 3.7 wt% and 1.5 wt% respectively, based on the standard inductively coupled plasma atomic emission spectrometer (ICP-AES) analysis. When the exposure time further increases to 70 s, metal atoms tend to aggregate into nanoparticles (Figure S7, Supporting Information). It is noted that the maximal loading of metal atoms achieved here is higher than the majority of SACs prepared via ALD in reported literatures.^[4,37,38]

To investigate the morphologies of as-prepared M_1/BP (Pd_1/BP and Pt_1/BP), high-resolution transmission electron microscopy measurements (HRTEM) and state-of-the-art aberration

C. H. Yao
Frontiers Science Center for Flexible Electronics (FSCFE)
Shaanxi Institute of Flexible Electronics (SIFE) & Shaanxi Institute of Biomedical Materials and Engineering (SIBME)
Northwestern Polytechnical University (NPU)
127 West Youyi Road, Xi'an 710072, China
S. J. Pennycook
Department of Materials Science & Engineering
National University of Singapore
9 Engineering Drive 1, Singapore 117575, Singapore
M. Lin
Institute of Materials Research and Engineering
Agency for Science, Technology and Research (A*STAR)
2 Fusionopolis Way, Innovis, #08-03, Singapore 138634, Singapore
E-mail: m-lin@imre.a-star.edu.sg

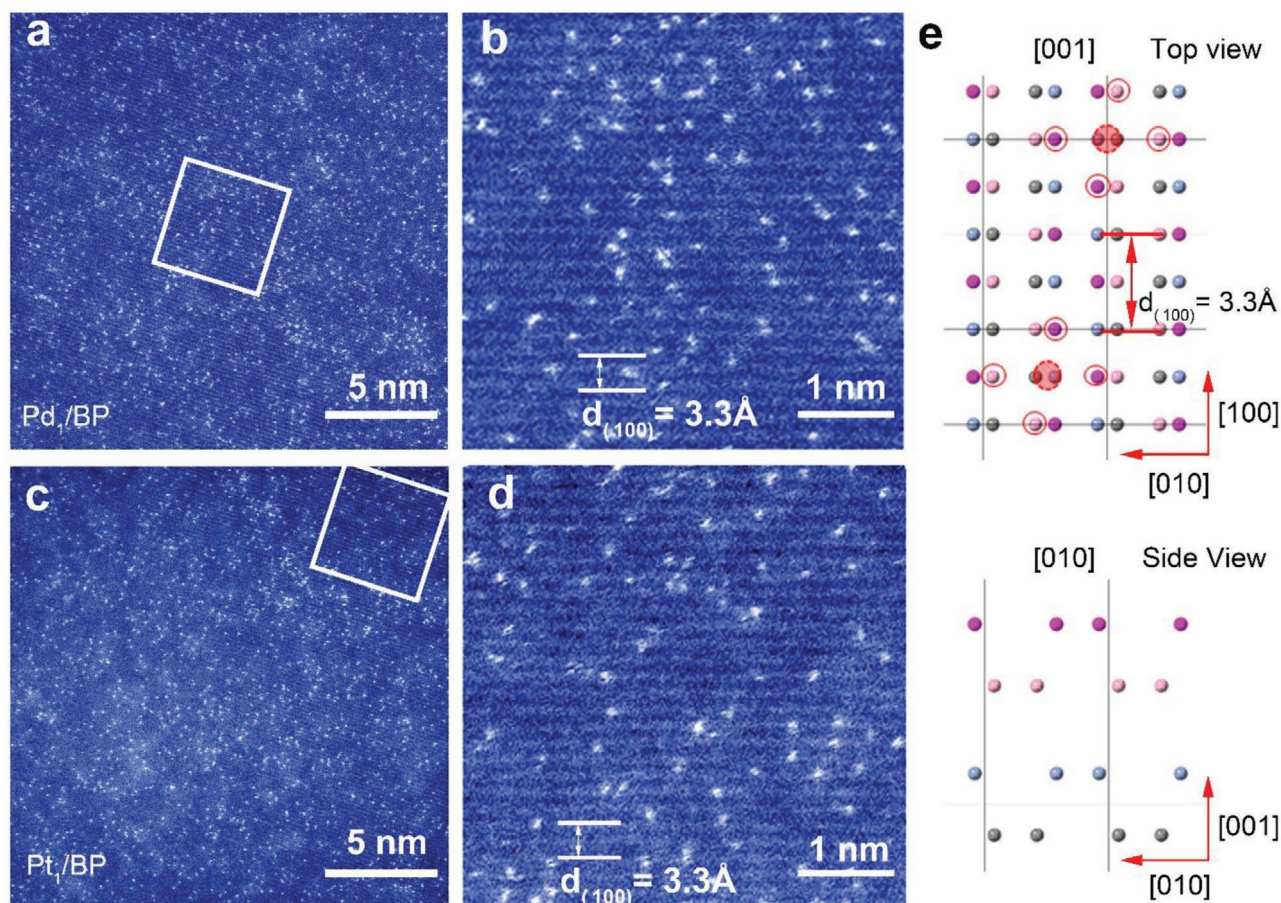


Figure 2. STEM characterization of Pd₁/BP and Pt₁/BP SACs. Aberration-corrected HAADF-STEM images of a,b) Pd₁/BP, c,d) Pt₁/BP; e) The simulated image of M₁/BP atomic model corresponding to the zigzag lattice plane of STEM images (b,d). The dashed red circle and the four hollow red circles around it highlight the possible adsorption site of single metal atoms over the vacancy site of BP along zigzag lattices and the P atoms connected to the single metal atom. Red, pink, blue and gray balls represent the first, second, third, and fourth layer of BP crystal.

corrected scanning transmission electron microscopy—annular dark field (STEM-ADF) were conducted. To avoid the beam damage of atomically thin BP flakes, 60 kV acceleration voltage was employed in all STEM experiments. Large-field view TEM and STEM images under bright field and dark field modes (Figures S8–S11, Supporting Information) reveal an absence of metal nanoparticles in both Pd₁/BP and Pt₁/BP samples. Instead, we observed a high density of isolated atoms uniformly dispersed on few-layer BP flakes (Figure 2a,c; Figures S9,S11, Supporting Information). Apart from the isolated metal atoms, the observation of BP lattice along the zigzag crystallographic orientation demonstrates that the crystallinity of BP host retains after ALD treatments, consistent with the Raman spectra of as-prepared Pd₁/BP SACs (Figure S12, Supporting Information). Interestingly, we found that most single metal atoms (both Pd and Pt) are located exactly at the zigzag lattice of BP with a zone axis [001] rather than randomly dispersed (Figure 2b,d). Figure 2e illustrate the corresponding zigzag lattice plane [001] with a lattice distance of 3.3 Å, wherein the solid red circle highlights the possible adsorption site of single metal atoms over the vacancy site of BP along zigzag lattices. This provides one piece of key information to validate the proposed atomic structure of M₁/BP SACs as discussed in a latter section. In addition,

the presence of a high density of atomically dispersed metal atoms on BP support is further confirmed by element mapping using energy-dispersive X-ray spectroscopy (Figures S13,S14, Supporting Information). These observations reveal that BP acts a promising 2D support to anchor a high density of single-metal atoms for catalysis.

In order to probe the local structure and valence state of single-metal atoms on BP, we performed X-ray absorption near-edge structure spectroscopy (XANES) and extended X-ray absorption fine structure spectroscopy (EXAFS) measurements of both Pd₁/BP and Pt₁/BP SACs (Figure 3). Figure 3a shows the normalized Pd K-edge XANES spectra of as-prepared Pd₁/BP, Pd foil, and PdO as the reference samples. The pre-edge adsorption acquired over Pd₁/BP resembles that of Pd foil, suggesting that Pd atoms in Pd₁/BP adopt a zero-valent state, presumably attributed to the fact that Pd and P have a similar electronegativity.^[39] In addition, the white line intensity of Pd₁/BP is much weaker than that of PdO, which further confirms its metallic-like valence state of Pd atoms. In contrast, Pt atoms in Pt₁/BP show a high valence state as confirmed by the Pt L3-edge XANES spectroscopic study (Figure 3d). The white line peak of Pt₁/BP is located at 11 568.9 eV, close to that of PtO₂ (11 569.5 eV) but higher than that of Pt foil (11 566 eV).

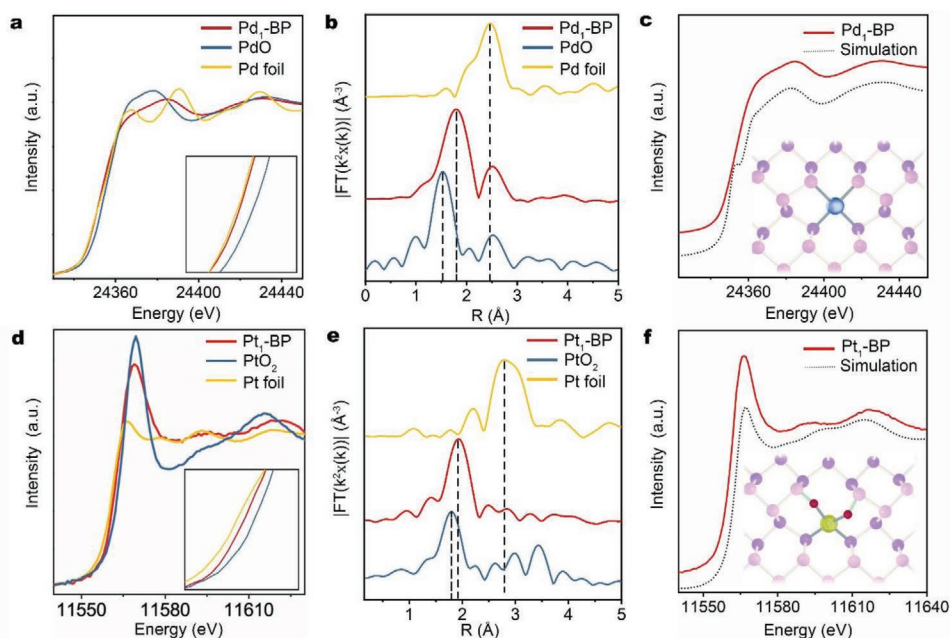


Figure 3. Local structural characterization of Pd₁/BP and Pt₁/BP SACs via XANES and EXAFS. a) Pd K-edge XANES spectrum and b) Fourier transform (FT) EXAFS of Pd₁/BP, PdO, and Pd foil respectively. c) Comparison of the experimental Pd K-edge XANES spectrum of Pd₁/BP (red line) with that of the simulated spectrum (black dot-line) of DFT-modelled structure (inset). d) Pt L3-edge XANES spectrum and e) Fourier transform (FT) EXAFS of Pt₁/BP, PtO₂, and Pt foil respectively. f) Comparison of the experimental Pt L3-edge XANES spectrum of Pt₁/BP (red line) with that of the simulated spectrum (black dot-line) of DFT-modelled structure (inset).

This indicates that Pt in Pt₁/BP exhibits a high oxidation state, although the electro-negativity of Pt is similar to that of Pd and P.^[38] Such a different behavior between Pt and Pd is ascribed to a high oxidation tendency of Pt precursors introduced by O₃, since the Pt precursor is unstable and easily oxidized, especially when organic ligands are removed.^[4] In order to probe the local structure of both Pd and Pt SACs, we further analyzed the R-space Fourier transform (FT) k³ EXAFS spectra of these two samples (Figure 3b and 3e). A prominent peak located at 1.7 Å in the spectrum of Pd₁/BP can be assigned to the Pd–P bonds, different from Pd–O and Pd–Pd bonds situated at 1.5 Å (PdO) and 2.5 Å (Pd foil), respectively.^[7] By contrast, Pt₁/BP shows a dominant peak around 1.9 Å, different from that of Pt–O bond (1.6 Å) in PtO₂ and Pt–Pt bond (2.6 Å) in Pt foils. Such a feature can be tentatively attributed to the co-existence of Pt–P and Pt–O bonds. The absence of metal-metal bond related features in both EXAFS spectra of Pd₁ and Pt₁ BP suggests the atomic dispersion of metal atoms on BP substrate, in line with the STEM results. In addition, X-ray photoelectron spectroscopy (XPS) results also suggest the presence of metallic-like Pd in Pd₁/BP, while the Pt in Pt₁/BP shows a high oxidation state between +2 to +4 (refer to Section S2, Supporting Information, for details).^[40,41]

To further probe the atomic structures of both Pd₁/BP and Pt₁/BP SACs, we performed the simulation of the XANES spectrum of DFT-relaxed atomic structures in comparison with experimental data (Figure 3c,f). A few structures for both Pd₁/BP and Pt₁/BP were proposed based on atomic lattice imaged STEM, the coordination number and bonding length as determined by the standard spectrum fitting (Section S3, Supporting Information). A throughout analysis reveals that Pd atom

confined in the DV of BP to form four Pd–P bonds (inset of Figure 3c) shows excellent agreement between experimental XANES data and simulated one. In contrast, the experiment XANES spectrum and simulated one of Pt bonded with four P atoms in DV (Section S3, Supporting Information) shows a large discrepancy. Instead, inserting two oxygen atoms into the local coordination structure to form P₂–Pt–O₂–P₂ yields good agreement between simulated and experimental data (inset of Figure 3f). These observations further attest the validity of the proposed atomic structures for both Pd₁ and Pt₁ SACs, consistent with their valence states, and atomic structures imaged by STEM. The zero-valent Pd SACs is expected to facilitate the hydrogenation reactions for organic transformations.

The selective hydrogenation is of fundamental importance for the styrene production as the footstone of olefin industrial materials.^[42] Therefore, we tested the catalytic performance of Pd₁/BP for the selective hydrogenation of various substituted phenylacetylenes (Figure 4). It turns out that Pd₁/BP exhibits an extremely high conversion and selectivity for semi-hydrogenation toward the formation of styrene and its derivatives (4 h, 80 °C, and 2 bar pressure), outperforming the catalytic activities of Pt₁/BP SACs and Pd nanoparticle counterparts. A number of reactive arene substituents including *para*-bromine and *para*-chlorine groups are tolerated. In addition, similar selectivity and reactivity results were obtained for the aliphatic alkyne substrate. As shown in Figure 4a,b, Pd₁/BP SAC delivers a conversion of 95%, 100%, 100%, and 100% as well as selectivity of 94%, 98%, 93%, and 99% for the selective hydrogenation of phenylacetylene to styrene, 4-bromophenylacetylene to 4-bromostyrene, methyl 4-ethynylbenzoate to methyl 4-vinylbenzoate, and 3-butylnylbenzene to 3-butenylbenzene, respectively.

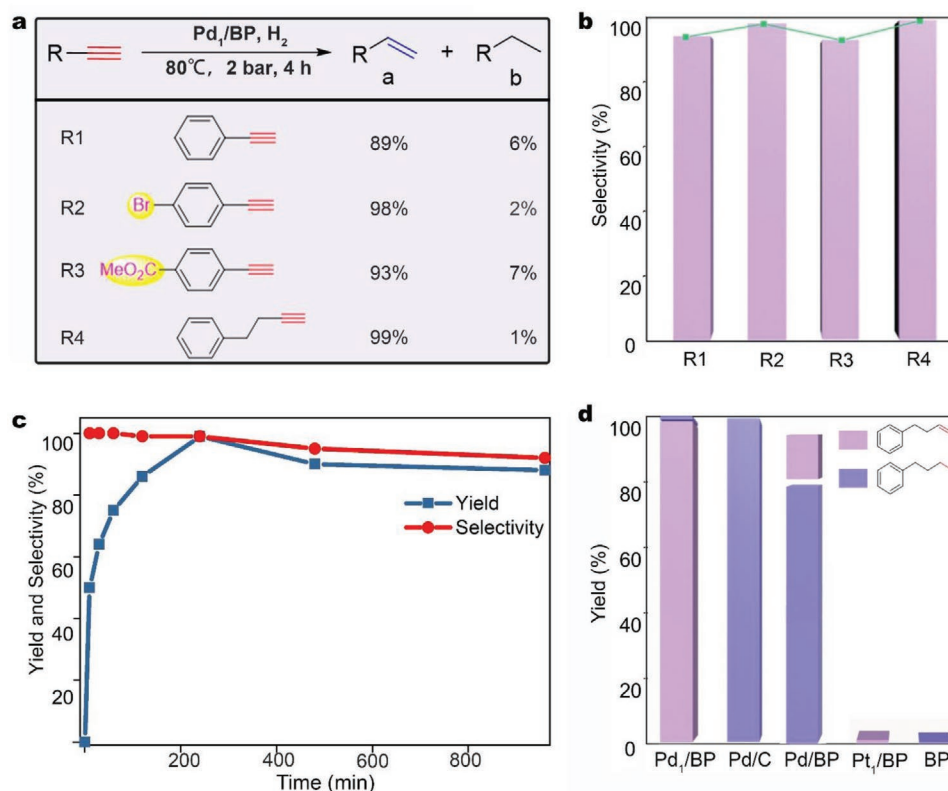


Figure 4. The evaluation of catalytic performance of Pd₁/BP SACs in semi-hydrogenation reaction. a,b) The catalytic performance (yield and selectivity) of Pd₁/BP (loading 1.5 wt%) for semi-hydrogenation reactions from phenylacetylene (R1) to styrene, 4-bromophenylacetylene (R2) to 4-bromostyrene, methyl 4-ethynylbenzoate (R3) to methyl 4-vinylbenzoate, and 3-butynylbenzene (R4) to 3-butenylbenzene, respectively. c) The plot of yield and selectivity versus time with Pd₁/BP (loading 1.5 wt%) for semi-hydrogenation reactions from 3-butynylbenzene (R4) to 3-butenylbenzene. d) The yield of the partial hydrogenation of 3-butynylbenzene to 3-butenylbenzene using Pd₁/BP SACs in compared to that of commercial Pd/C, Pd nanoparticles on BP (Pd/BP), bare BP nanosheets, and Pt₁/BP SACs.

Furthermore, to better evaluate the reaction rate and selectivity of Pd₁/BP SAC, semi-hydrogenation reactions were carried out to monitor the formation of alkene as a function of time ranging from 10 to 960 min. As shown in Figure 4c, 50% alkene, and 99% conversion and 99% alkene can be achieved within 10 min and 4 h, respectively. In addition, more than 90% alkene has been obtained even under the prolonged reaction time of 16 h. In the presence of a mixture of alkyne and alkene (e.g., 3-butynylbenzene and 3-butenylbenzene), Pd₁/BP also demonstrated a high selectivity of 95% and 99% conversion in the partial hydrogenation of 3-butynylbenzene to 3-butenylbenzene. The stability of Pd₁/BP catalyst was also evaluated by extending the semi-hydrogenation reaction from 4 to 16 h with an increase of reactants loading by four times (note that the amount of Pd₁/BP catalyst [10 mg] and reaction condition [80 °C and 2 bar]) were kept the same. Under these conditions, Pd₁/BP SAC delivers a 99% conversion and 88% selectivity of 3-butynylbenzene. Furthermore, the recycled Pd₁/BP SAC also delivers a 99% conversion and 75% selectivity. Thus, Pd₁/BP catalyst shows a fairly good activity, stability, and recyclability. In addition, Pd nanoparticle on BP, Pd/C, Pt₁/BP SACs, or bare BP show either no or poor selectivity (<5%) for semi-hydrogenation of 3-butynylbenzene to 3-butenylbenzene (Figure 4d). In addition, the excellent atomic dispersion of as-prepared Pd₁/BP

SACs (0.3 wt%, 0.6 wt%, 1.5 wt%) results in a reasonably high turnover frequency (TOF) of 0.3 s⁻¹ in the semi-hydrogenations of 3-butynylbenzene (Table S2, Supporting Information).^[43–50] It is worth mentioning that little aggregated Pd atoms in Pd₁/BP after the hydrogenation reactions suggest atomic dispersion of single metal atoms on BP can be maintained (Figure S30, Supporting Information).

We then performed DFT calculations to probe the underlying mechanism for superior catalytic performance of zero-valent Pd₁/BP for the selective semi-hydrogenation reactions. In our calculations, we considered 4-bromophenylacetylene as the prototypical reactant, which would be referred to as C1. Prior to the mechanistic study of the selective hydrogenation, the charge redistribution upon the chemisorption of Pd atom in the divacancy of BP was calculated and plotted in Figure 5a. Although the very similar electronegativities between Pd and P did not result in any significant charge transfer, it induced a local change in the chemical properties of the material, which would be pivotal in the selective hydrogenation reaction. The P atoms surrounding the Pd would be expected to be chemically different from the rest. Next, we studied the H₂ adsorption on Pd₁/BP and found that, surprisingly, H₂, as a molecule, does not tend to adsorb on the Pd atom nor the surrounding P atoms. Instead, our calculations suggested that

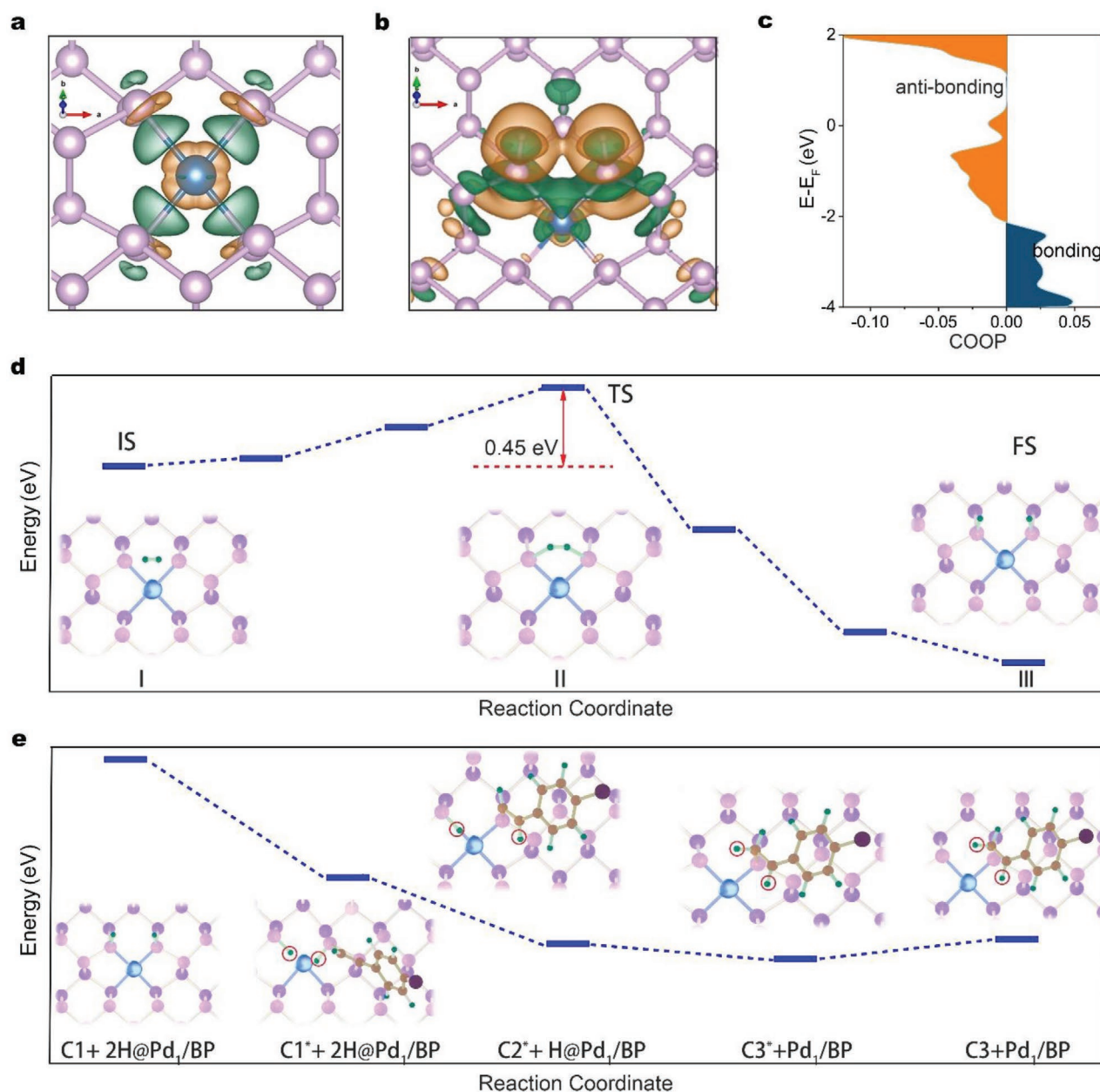


Figure 5. Investigation of the catalytic origin over BP supported SACs. Isosurface of the charge redistribution a) upon adsorption of a Pd atom in the DV of BP, and b) upon dissociative adsorption of H₂ on Pd₁/BP. Note that the dark green (orange) region represents electron accumulation (depletion) respectively. c) The COOP plot for the Pd–P interactions in a Pd₁/BP unit cell. By convention, positive (negative) region indicates (anti-)bonding interactions. From the plot, antibonding interactions dominate around E_F. d) The relative energy of the dissociative adsorption of H₂ over Pd₁/BP. e) The relative energy of the hydrogenation of 4-bromophenylacetylene reactions including reactants, intermediates, and products over Pd₁/BP.

the H₂ should undergo dissociative adsorption on the BP surface. In Figure 5d, we plotted the mechanistic pathway of the H₂ dissociative adsorption and revealed that the energy barrier amounted to only 0.49 eV (from initial state I to transition state II), indicating that the reaction can happen even at ambient conditions. Such a low energy barrier is made possible by the simultaneous formation of the P–H bonds and the dissociation of the H–H bond during the transition state, in which the P–H bond decreases from 3.31 to 1.95 Å and the H–H bond increases from 0.75 to 0.86 Å respectively.

Furthermore, this dissociative adsorption proceeded exothermically, releasing the energy of 1.20 eV (from initial state I to final state III).

Upon dissociative H₂ adsorption, Pd remains nearly zero valence state, while the H atoms gain 0.3 |e| each and the P atoms that the H atoms bonded with lost 0.4 |e|. Such electron transfer would originate from the Pd–P bonds, as suggested from the charge redistribution plot as shown in Figure 5b. In fact, it was found that the Pd–P bonds shorten from 2.41 to 2.32 Å upon dissociative H₂ adsorption. This can

be rationalized by the fact that the electrons gained by H atoms originate from the antibonding interactions between Pd–P in Pd₁/BP, as shown from the COOP (crystal orbital overlap population) plot for Pd–P interactions in Figure 5c that antibonding interactions dominate around Fermi level (E_F). Note that according to convention, the positive values of COOP would indicate bonding interactions while negative values indicate antibonding interactions. After the adsorption, the calculated integrated COHP (ICOHP) (crystal orbital Hamilton population) up to E_F for the Pd–P interactions decreased from –1.85 to –2.10 eV, indicating the enhanced stabilization of the Pd–P interactions due to the reduction of the antibonding interactions, in which the electrons were to be transferred to the H atoms.

With the pre-adsorbed H atoms from the dissociative adsorption of H₂, the energies of the elementary step of the selective hydrogenation of C1 were evaluated and plotted in Figure 5e. C1 can co-adsorb on the hydrogenated BP exothermically releasing the energy of 0.61 eV by breaking one of the π bonds of the C–C triple bond and forming C–P bonds. We found that every step is exothermic except for the last step, which is the desorption of C3. Nevertheless, the desorption would only require 0.13 eV from our calculations. As such, C3 readily desorbs from the surface without undergoing the full hydrogenation to alkane. In addition, C3 only co-adsorb over the hydrogenated BP with an adsorption energy of magnitude less than 0.1 eV (–0.07 eV), indicating that C3 would not tend to compete with C1 in the co-adsorption. This weak interaction between BP and C3 shall be the cause of the selectivity in semi-hydrogenation reaction.

In comparison with Pd nanoclusters, both C1 and C3 adsorbs highly exothermically on Pd (111) surface (Figure S31, Supporting Information), releasing more than 2.0 eV (adsorption energy of C1 on Pd (111) was –2.60 eV and that of C3 was –2.26 eV). Hence, it would be expected that after the hydrogenation of C1 to C3, C3 would not leave the Pd surface but would continue with the hydrogenation till it forms the alkane final product.

3. Conclusions

In summary, we have successfully demonstrated a novel approach for a controllable synthesis of high-density Pd₁ and Pt₁/SACs confined on the surface of BP via ALD process. Unlike other flat 2D materials, the buckled BP surface acts as a giant phosphorus ligand to confine zero-valent single-metal atoms via metal phosphorus interactions. Interestingly, Pd₁/BP with zero-valent state shows a superior conversion (100%) and selectivity (99%) in the selective partial hydrogenation of phenylacetylene and its derivatives to the corresponding styrenes. The synthesis of zero-valent SACs on BP with peculiar electronic and catalytic properties opens new opportunities for industrially important chemical transformations.

Supporting Information

Supporting Information is available from the Wiley Online Library or from the author.

Acknowledgements

C.C., W.O., K.M.Y., and S.B.X. contributed equally to this work. J.L. acknowledges the support from MOE grants (MOE2019-T2-2-044 and R-143-000-B47-114) and the support from Agency for Science, Technology and Research (A*STAR) under its AME IRG Grant (Project No. A20E5c0096). C.Z. thanks the support of the MOE grant (R-723-000-029-112) and NUS Green Energy Program (R-143-000-A63-114). This research used resources of the 7-BM Beamline of the National Synchrotron Light Source II, a U.S. Department of Energy (DOE) Office of Science User Facility operated for the DOE Office of Science by Brookhaven National Laboratory under Contract No. DE-SC0012704. Thanks for the support of Electron Microscopy Center, Shenzhen University. Computational works were performed at the NUS Graphene Research Centre computing cluster facilities. X.X.Z. thanks the support from the Presidential Postdoctoral Fellowship, Nanyang Technological University, Singapore via grant 03INS000973C150. C.L.S. thanks the support from Shenzhen Peacock Plan (KQTD2016053112042971), Shenzhen Innovation Program (JCYJ20190808142001745, RCJC20200714114434086), and Pengcheng Scholar Program.

Conflict of Interest

The authors declare no conflict of interest.

Data Availability Statement

The data that support the findings of this study are available from the corresponding author upon reasonable request.

Keywords

black phosphorus, reaction mechanisms, single-atom catalysts, zero valence

Received: December 15, 2020

Revised: April 21, 2021

Published online:

- [1] B. Qiao, A. Wang, X. Yang, L. F. Allard, Z. Jiang, Y. Cui, J. Liu, J. Li, T. Zhang, *Nat. Chem.* **2011**, 3, 634.
- [2] X.-F. Yang, A. Wang, B. Qiao, J. Li, J. Liu, T. Zhang, *Acc. Chem. Res.* **2013**, 46, 1740.
- [3] J. Lin, A. Wang, B. Qiao, X. Liu, X. Yang, X. Wang, J. Liang, J. Li, J. Liu, T. Zhang, *J. Am. Chem. Soc.* **2013**, 135, 15314.
- [4] S. Sun, G. Zhang, N. Gauquelin, N. Chen, J. Zhou, S. Yang, W. Chen, X. Meng, D. Geng, M. N. Banis, *Sci. Rep.* **2013**, 3, 1775.
- [5] K. Ding, A. Gulec, A. M. Johnson, N. M. Schweitzer, G. D. Stucky, L. D. Marks, P. C. Stair, *Science* **2015**, 350, 189.
- [6] H. Wei, X. Liu, A. Wang, L. Zhang, B. Qiao, X. Yang, Y. Huang, S. Miao, J. Liu, T. Zhang, *Nat. Commun.* **2014**, 5, 5634.
- [7] H. Yan, H. Cheng, H. Yi, Y. Lin, T. Yao, C. Wang, J. Li, S. Wei, J. Lu, *J. Am. Chem. Soc.* **2015**, 137, 10484.
- [8] A. Wang, J. Li, T. Zhang, *Nat. Rev. Chem.* **2018**, 2, 65.
- [9] M. Yang, L. F. Allard, M. Flytzani-Stephanopoulos, *J. Am. Chem. Soc.* **2013**, 135, 3768.
- [10] X. Hai, X. Zhao, N. Guo, C. Yao, C. Chen, W. Liu, Y. Du, H. Yan, J. Li, Z. Chen, *ACS Catal.* **2020**, 10, 5862.
- [11] H. Zhang, J. Li, S. Xi, Y. Du, X. Hai, J. Wang, H. Xu, G. Wu, J. Zhang, J. Lu, *Angew. Chem.* **2019**, 131, 15013.

- [12] H. Yan, X. Zhao, N. Guo, Z. Lyu, Y. Du, S. Xi, R. Guo, C. Chen, Z. Chen, W. Liu, *Nat. Commun.* **2018**, 9, 1.
- [13] L. Lin, S. Yao, R. Gao, X. Liang, Q. Yu, Y. Deng, J. Liu, M. Peng, Z. Jiang, S. Li, *Nat. Nanotechnol.* **2019**, 14, 354.
- [14] Z. Chen, E. Vorobyeva, S. Mitchell, E. Fako, M. A. Ortuño, N. López, S. M. Collins, P. A. Midgley, S. Richard, G. Vilé, *Nat. Nanotechnol.* **2018**, 13, 702.
- [15] S. K. Kaiser, Z. Chen, D. Faust Akl, S. Mitchell, J. Pérez-Ramírez, *Chem. Rev.* **2020**, 120, 11703.
- [16] X. Wang, W. Chen, L. Zhang, T. Yao, W. Liu, Y. Lin, H. Ju, J. Dong, L. Zheng, W. Yan, *J. Am. Chem. Soc.* **2017**, 139, 9419.
- [17] G. Vilé, D. Albani, M. Nachttegaal, Z. Chen, D. Dontsova, M. Antonietti, N. López, J. Pérez-Ramírez, *Angew. Chem., Int. Ed.* **2015**, 54, 11265.
- [18] N. Cheng, S. Stambula, D. Wang, M. N. Banis, J. Liu, A. Riese, B. Xiao, R. Li, T.-K. Sham, L.-M. Liu, G. A. Botton, X. Sun, *Nat. Commun.* **2016**, 7, 13638.
- [19] A. Bakandritsos, R. G. Kadam, P. Kumar, G. Zoppellaro, M. Medved, J. Tuček, T. Montini, O. Tomanec, P. Andrášková, B. Drahoš, *Adv. Mater.* **2019**, 31, 1900323.
- [20] H. B. Yang, S.-F. Hung, S. Liu, K. Yuan, S. Miao, L. Zhang, X. Huang, H.-Y. Wang, W. Cai, R. Chen, *Nat. Energy* **2018**, 3, 140.
- [21] G. Pacchioni, P. S. Bagus, *Inorg. Chem.* **1992**, 31, 4391.
- [22] L. M. Pignolet, *Homogeneous Catalysis with Metal Phosphine Complexes*, Springer Science & Business Media, New York **2013**.
- [23] H. Watanabe, M. Kobayashi, K. Higuchi, *J. Organomet. Chem.* **1980**, 186, 51.
- [24] I. Kmentová, B. Gotov, E. Solcániová, Š. Toma, *Green Chem.* **2002**, 4, 103.
- [25] S. Tauster, S. Fung, R. L. Garten, *J. Am. Chem. Soc.* **1978**, 100, 170.
- [26] T. W. van Deelen, C. H. Mejía, K. P. de Jong, *Nat. Catal.* **2019**, 2, 955.
- [27] P. Hu, Z. Huang, Z. Amghouz, M. Makkee, F. Xu, F. Kapteijn, A. Dikhtiarenko, Y. Chen, X. Gu, X. Tang, *Angew. Chem., Int. Ed.* **2014**, 53, 3418.
- [28] A. Morita, *Appl. Phys. A* **1986**, 39, 227.
- [29] H. Yan, Y. Lin, H. Wu, W. Zhang, Z. Sun, H. Cheng, W. Liu, C. Wang, J. Li, X. Huang, *Nat. Commun.* **2017**, 8, 1.
- [30] C. Marichy, M. Bechelany, N. Pinna, *Adv. Mater.* **2012**, 24, 1017.
- [31] J. Li, C. Chen, S. Liu, J. Lu, W. P. Goh, H. Fang, Z. Qiu, B. Tian, Z. Chen, C. Yao, *Chem. Mater.* **2018**, 30, 2742.
- [32] Y. Guo, J. Robertson, *Sci. Rep.* **2015**, 5, 14165.
- [33] J. Gaberle, A. L. Shluger, *Nanoscale* **2018**, 10, 19536.
- [34] L. Cao, W. Liu, Q. Luo, R. Yin, B. Wang, J. Weissenrieder, M. Soldemo, H. Yan, Y. Lin, Z. Sun, *Nature* **2019**, 565, 631.
- [35] R. L. Puurunen, *Chem. Vap. Deposition* **2003**, 9, 249.
- [36] J. S. King, A. Wittstock, J. Biener, S. O. Kucheyev, Y. M. Wang, T. F. Baumann, S. K. Giri, A. V. Hamza, M. Baeumer, S. F. Bent, *Nano Lett.* **2008**, 8, 2405.
- [37] Y. Ren, Y. Tang, L. Zhang, X. Liu, L. Li, S. Miao, D. S. Su, A. Wang, J. Li, T. Zhang, *Nat. Commun.* **2019**, 10, 1.
- [38] H. Yan, Y. Lin, H. Wu, W. Zhang, Z. Sun, H. Cheng, W. Liu, C. Wang, J. Li, X. Huang, *Nat. Commun.* **2017**, 8, 1070.
- [39] J. C. Boeyens, *Zeitschrift für Naturforsch., B* **2008**, 63, 199.
- [40] Y. Ma, H. Wang, H. Li, J. Key, S. Ji, R. Wang, *RSC Adv.* **2014**, 4, 20722.
- [41] L. Bai, X. Wang, S. Tang, Y. Kang, J. Wang, Y. Yu, Z. K. Zhou, C. Ma, X. Zhang, J. Jiang, *Adv. Mater.* **2018**, 30, 1803641.
- [42] Q. Fan, S. He, L. Hao, X. Liu, Y. Zhu, S. Xu, F. Zhang, *Sci. Rep.* **2017**, 7, 42172.
- [43] D. Deng, Y. Yang, Y. Gong, Y. Li, X. Xu, Y. Wang, *Green Chem.* **2013**, 15, 2525.
- [44] J.-W. Yu, X.-Y. Wang, C.-Y. Yuan, W.-Z. Li, Y.-H. Wang, Y.-W. Zhang, *Nanoscale* **2018**, 10, 6936.
- [45] S. Song, K. Li, J. Pan, F. Wang, J. Li, J. Feng, S. Yao, X. Ge, X. Wang, H. Zhang, *Adv. Mater.* **2017**, 29, 1605332.
- [46] Z.-S. Wang, C.-L. Yang, S.-L. Xu, H. Nan, S.-C. Shen, H.-W. Liang, *Inorg. Chem.* **2020**, 59, 5694.
- [47] Q. Feng, S. Zhao, Y. Wang, J. Dong, W. Chen, D. He, D. Wang, J. Yang, Y. Zhu, H. Zhu, L. Gu, Z. Li, Y. Liu, R. Yu, J. Li, Y. Li, *J. Am. Chem. Soc.* **2017**, 139, 7294.
- [48] J. Liu, J. Shan, F. R. Lucci, S. Cao, E. C. H. Sykes, M. Flytzani-Stephanopoulos, *Catal. Sci. Technol.* **2017**, 7, 4276.
- [49] C. Riley, S. Zhou, D. Kunwar, A. De La Riva, E. Peterson, R. Payne, L. Gao, S. Lin, H. Guo, A. Datye, *J. Am. Chem. Soc.* **2018**, 140, 12964.
- [50] G. X. Pei, X. Y. Liu, X. Yang, L. Zhang, A. Wang, L. Li, H. Wang, X. Wang, T. Zhang, *ACS Catal.* **2017**, 7, 1491.